



Article

# Effect of Flashlamp Heating System Parameters on the Wedge Peel Strength of Thermoplastic Carbon Fiber Tape in the Automated Tape Placement Process

Alexander Legenstein and Ewald Fauster \*

Processing of Composites and Design for Recycling, Montanuniversität Leoben, 8700 Leoben, Austria;  
alexander.legenstein@unileoben.ac.at

\* Correspondence: ewald.fauster@unileoben.ac.at

**Abstract:** Laser-assisted automated tape placement systems are currently the state of the art regarding thermoplastic tape placement. Flashlamp heating systems are rather new in this field of application and offer high energy density with low safety requirements and moderate costs compared to laser-assisted automated tape placement systems. In this study, the effect of processing parameters on interlaminar bonding of carbon fiber-reinforced polyamide 6 tapes is investigated using a flashlamp heating system. The temperature during placement is monitored using an infrared camera, and the bonding strength is characterized by a wedge peel test. The bonding quality of the tapes placed between 210 °C and 330 °C at a lay-up speed of 50 mm/s is investigated. Thermogravimetric analysis, differential scanning calorimetry, and micrographs are used to investigate the material properties and effects of the processing conditions on the thermophysical properties and geometric properties of the tape. No significant changes in the thermophysical or geometric properties were found. Moisture within the tapes and staining of the quartz guides of the flashlamp system have significant influence on the bonding strength. The highest wedge peel strength of dried tapes was found at around 330 °C.

**Keywords:** automated tape placement; thermoplastic resin; bonding; polymer matrix composites; material characterization



**Citation:** Legenstein, A.; Fauster, E. Effect of Flashlamp Heating System Parameters on the Wedge Peel Strength of Thermoplastic Carbon Fiber Tape in the Automated Tape Placement Process. *J. Manuf. Mater. Process.* **2024**, *8*, 91. <https://doi.org/10.3390/jmmp8030091>

Academic Editors: Patricia Krawczak and Ludwig Cardon

Received: 21 March 2024

Revised: 23 April 2024

Accepted: 24 April 2024

Published: 29 April 2024



**Copyright:** © 2024 by the authors. Licensee MDPI, Basel, Switzerland. This article is an open access article distributed under the terms and conditions of the Creative Commons Attribution (CC BY) license (<https://creativecommons.org/licenses/by/4.0/>).

## 1. Introduction

Automated Tape Placement (ATP) can be used to manufacture lightweight and high-performance composites structures in a single-step process using thermoplastic polymer matrix composite materials. ATP in this context is defined as the automated positional- and directional-variable placement of a single unidirectional reinforced prepregged polymer tape on flat or curved surfaces with defined laminate thickness [1]. This methodology does not require an autoclave cycle and is therefore faster, cleaner, and more energy efficient compared to thermoset ATP processes. This is particularly of interest in the aerospace industry, as the autoclave limits the dimensions of the part that can be manufactured [2,3]. Thermoplastic polymers not only help with realizing broader design spaces; they are also easier to repair and recycle compared to thermoset polymers due to their ability to be remelted. Thermoset polymers are brittle and are irreversibly crosslinked. Thermoplastic polymers are already fully polymerized in their resin state and do not exhibit crosslinking. The structural stability is achieved by enabling the polymer chains to move at high temperature and form entangled structures [4]. Most research on thermoplastics polymers for ATP focuses on high-performance matrix materials such as PEEK [4–20], PEKK [21–23], or PPS [24–27]. Engineering or commodity thermoplastics have received far less attention within the recent years. Some studies exist investigating PA6 [16,28–30], PA66 [31], PA12 [32,33], or PP [34–37]. Low-cost thermoplastic matrix systems are particularly of interest for cost-sensitive and high-volume industries such as the automotive sector [38],

as they offer easy processability, high toughness, damage tolerance, and better recyclability compared to thermoset structures [39]. The most common methods of processing fiber-reinforced thermoplastic tapes with ATP are with laser [5,8,10,12,13] or hot gas torch heating systems [6,7,40–44]. Hot gas torch heating systems have a low energy density and long response time compared to laser systems. This limits the possible processing speed and restrains the design space. Laser systems come with higher equipment costs and need to be in an isolated room to guarantee safety [45]. Flashlamp systems can bridge the gap between hot gas torch and laser heating systems for thermoplastic ATP. These systems are based on pulsed light technology and utilize high-energy pulsed flashes for heating the tapes. A high voltage is used to ionize the xenon gas in the lamp to conduct electricity. The capacitors are discharged at regular intervals to generate flashes. These flashes deliver the heat to the target. Quartz guides are used as an optical medium to focus the flashes. Based on the geometry of the quartz, the energy can be distributed between the incoming tape and the substrate. These systems have lower acquisition and operation costs, as well as safety requirements, while offering equal power as laser systems [46,47]. Research on flashlamp systems is currently limited to reflectivity and emissivity analyses of composites heated by those systems [48], thus benchmarking those systems for CF/PPS [49] or facilitating the development of heat transfer models for dry fiber and thermoplastic materials [46,50]. Pulsed operation of the flashlamp system can cause high levels of material temperature (above the thermal degradation threshold of the materials) [46]. This effect could influence the bonding strength of the laminate. Especially at complex geometries, local overheating can damage the matrix [51]. The bonding of thermoplastic materials is affected by the crystallinity level, the void content, or thermal degradation. All of those effects are dependent on the thermal history during processing. The process window for ATP needs to be defined precisely in order to guarantee high bonding quality and avoid altering the composite due to high temperature [52]. In ATP, small surface areas are typically heated with heat rates of up to 500 °C/s but with short exposure time (<0.2 s) depending on the placement speed [16]. High lay-up speeds need higher power inputs to sufficiently melt the matrix and bond the tapes. Furthermore, sufficient consolidation force is needed to ensure enough time for the molecular chains to reptate between the layers for optimal bonding [42]. Bonding occurs above the glass transition temperature ( $T_g$ ) for amorphous thermoplastics and above the melting temperature ( $T_m$ ) for crystalline polymers. However, the bonding of semicrystalline thermoplastics was also shown to occur below the melting point [53].

The work at hand aims to experimentally investigate the temperature distribution of unidirectional tapes during ATP with a flashlamp heating system. The temperature of the incoming tape was measured close to the nip point using an IR camera. Different processing conditions (pulse width and frequency of the heating system) were used to manufacture samples and evaluate the resulting temperature close to the nip point. The samples were made from unidirectional CF/PA6 tapes due to the low cost of this material compared to high-performance tapes (e.g., CF/PEEK) and the lack of ATP-based studies regarding CF/PA6, particularly with flashlamp heating. All samples consisted of four tape layers resulting in a  $[0]_4$  laminate, which in turn was used to determine the wedge peel strength. The moisture within the tapes was measured. The impact of different drying conditions on the wedge peel strength was tested. Thermogravimetric Analysis (TGA) was used to determine the degradation point of the investigated polymers, and Differential Scanning Calorimetry (DSC) was used to study the influence of processing conditions on the thermophysical properties of the polymers. The fiber–matrix distribution and the bonding interface were investigated with optical microscopy.

## 2. Materials and Methods

### 2.1. Materials

The material used for this study is a fully impregnated thermoplastic CF/PA6 tape from SGL Carbon SE (Sigapreg® TP C U157-0/NF-T340/46%) with a width of 25.4 mm and

a thickness of 0.2 mm. The fiber volume content is 42%, and the mass density is 1.42 g/cm<sup>3</sup>. The fiber type is Sigrafil® C T50-4.4/255-T140. The matrix has a melting temperature  $T_m$  of 220 °C and a  $T_g$  of 58 °C.

## 2.2. ATP System and Placement Trials

The ATP system used in this study is shown in Figure 1d and consists of a placement head with feeding unit, a silicone compaction roller with 70 Shore A hardness, 30 mm width, and a diameter of 50 mm. The setup is able to place 25.4 mm wide tapes on a heated aluminum tool measuring 700 mm × 350 mm. The tool can be heated with an accuracy of  $\pm 1$  °C.

The consolidation force was measured using a multicomponent sensor with an accuracy of 4 N and a resolution of 0.2 N. A hygrometer is used to measure room temperature and humidity. It was placed right next to the ATP rig and the material storage. The hygrometer has an accuracy of  $\pm 0.5$  °C and a resolution of 0.1% for the temperature measurement, whereas the humidity can be measured with an accuracy of  $\pm 3\%$  and a resolution of 0.1%. All placement trials were performed with a *Heraeus humm3* flashlamp system as heating source (see Figure 1c). The quartz guide has an angle of 23° to the substrate and a width of 30 mm. Two different chamfered quartz guides were used in this study. Figure 1a shows the geometry of a chamfered quartz guide with one radiating surface, and Figure 1b shows the geometry with three radiating surfaces. The configuration of the quartz guide in the processing environment is shown in Figure 1c,d. All tapes were placed directly on the aluminum tool. The tool was heated to 50 °C to ensure equal placement conditions for all trials. The lay-up speed was set to 50 mm/s, and the consolidation force was set to 500 N for all tests.

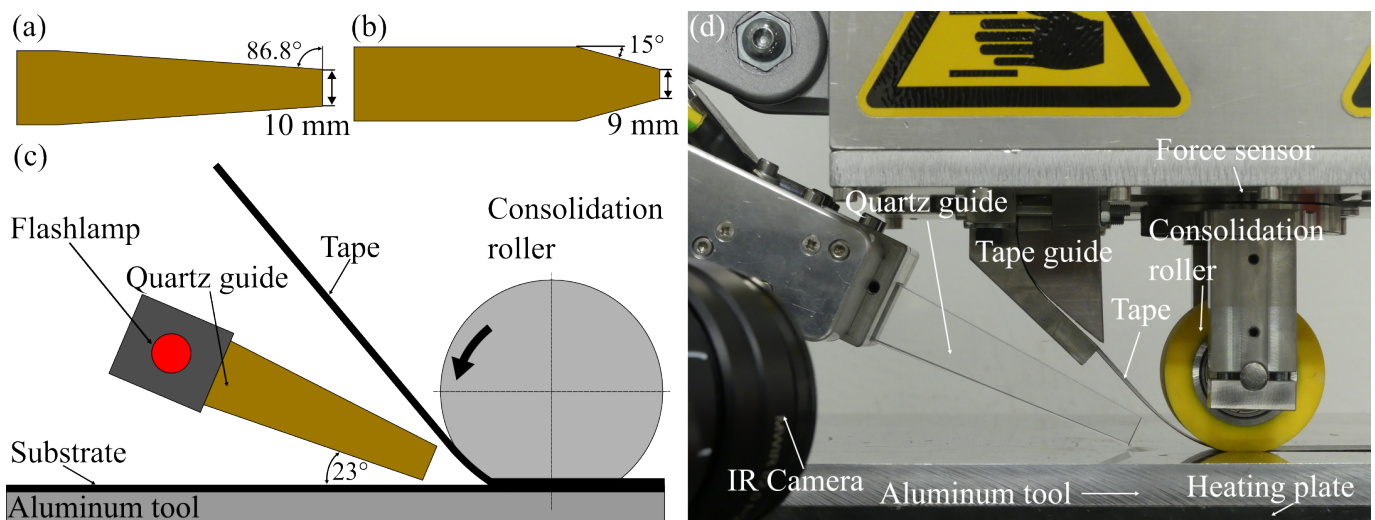


**Figure 1.** (a) Quartz with one radiating surface. (b) Quartz with three radiating surfaces. (c) Schematic of the flashlamp system placement within the ATP system. (d) ATP setup used in this study.

The samples for the peel test were manufactured at different flashlamp parameters as listed in Table 1. Three peel test samples were manufactured for each parameter configuration. For the first experimental set, the pulse width was kept constant, and for the other set, the frequency was kept constant. For both sets, the power was increased from around 2150 W to the maximum power setting of the flashlamp system (4400 W). To compare the temperature between the experimental sets, uniform power levels were chosen (ranging from 1 to 5, with 5 being the highest power setting, as shown in Table 1). The power levels differ with a maximum value of 26 W at the highest power setting.

**Table 1.** Experimental plan.

Exp. Set	Frequency [Hz]	Pulse Width [ $\mu$ s]	Power [W]	Power Level [-]
1	40	2200	2153	1
	50	2200	2691	2
	60	2200	3229	3
	70	2200	3767	4
	80	2200	4306	5
2	30	2950	2159	1
	30	3700	2676	2
	30	4550	3236	3
	30	5400	3779	4
	30	6200	4280	5

### 2.3. Temperature Measurement

In order to determine the associated temperature of the incoming tape for the parameter combinations shown in Table 1, a series of tapes was placed onto the aluminum tool to form a  $[0]_4$  laminate. The temperatures were measured on the incoming third layer due to the tapes being pulled apart between the second and third layer for the wedge peel test. The temperature of the incoming tape was measured using an InfraTec Image IR 8300 IR camera. The IR camera has a detector format of  $640 \times 512$  pixels with a temperature resolution of 0.025 K at 30 °C. The camera uses a lens with 25 mm focal length. The nip-point temperature cannot be measured directly with the IR camera. Combinations of surface emittance and specular reflections of the opposing surfaces near the nip point distort the temperature measurement [54]. Therefore, the temperature was measured closely before the nip point. It needs to be noted that the temperature could differ from the actual processing temperature, because it is not measured directly at the nip point. The emissivity was set to 0.91, as the values typically range from 0.8 to 0.95 depending on the material and the geometrical configuration of the setup [30].

### 2.4. Wedge Peel Strength Measurement System

The bonding quality of composite laminates are typically characterized by the crack propagation resistance with Double Cantilever Beam (DCB) tests for mode I and End Load Split (ELS) for mode II crack initiation [55]. Another common test method for evaluating of the bonding strength is the Short Beam Strength (SBS) test [4,21,53,56,57]. High-performance thermoplastics can be tested with SBS and show valid failure modes [4]. However, it was shown by Schaefer [58] that SBS tests on CF/PA6 result in wrong values, because the samples did not experience interlaminar crack formation and failed due to plastic shear. Stokes-Griffin et al. [16] also listed poor fiber–matrix bonding as a possible contributing factor for the failing test. Wedge peel tests have been widely used [13,16,18,59] to compare the interlaminar bonding of different composites and are an alternative to SBS or DCB tests for the evaluation of the bonding strength, as they show good correlation with DCB tests [60]. Although it is not yet standardized for this kind of test, wedge peel testing is conceptually comparable to standardized tests for adhesive bonding, e.g., ASTM D3762. The wedge peel test is able to continuously test the bonding strength over the whole sample length and is therefore suitable to identify any differences in bonding strength occurring from process conditions. Due to the noncontinuous heating behavior of the flashlamp system, different bonding levels over the length of the tape can occur. The peel test setup used for this study is shown in Figure 2. It consists of a wedge with a thickness of 10 mm and a wedge angle of 40°. The tip of the wedge is rounded and has a radius of 0.5 mm. All surfaces of the wedge have a mean roughness depth (difference between peak and valley height) of  $R_z = 0.63 \mu\text{m}$ . The tapes are pulled over the wedge with the interface in between the second and third ply. The peel speed was set to 1 mm/s. The peel force is measured by two load cells (located underneath the peel wedge) with a capacity of 300 N and a resolution of 0.009 N at an acquisition rate of 10 Hz. The sample width was measured

with a caliber at 10 points (same positions for each tape on the third layer) and averaged to calculate the arithmetic mean of the tape width. The digital caliber has a measurement accuracy of 0.03 mm.

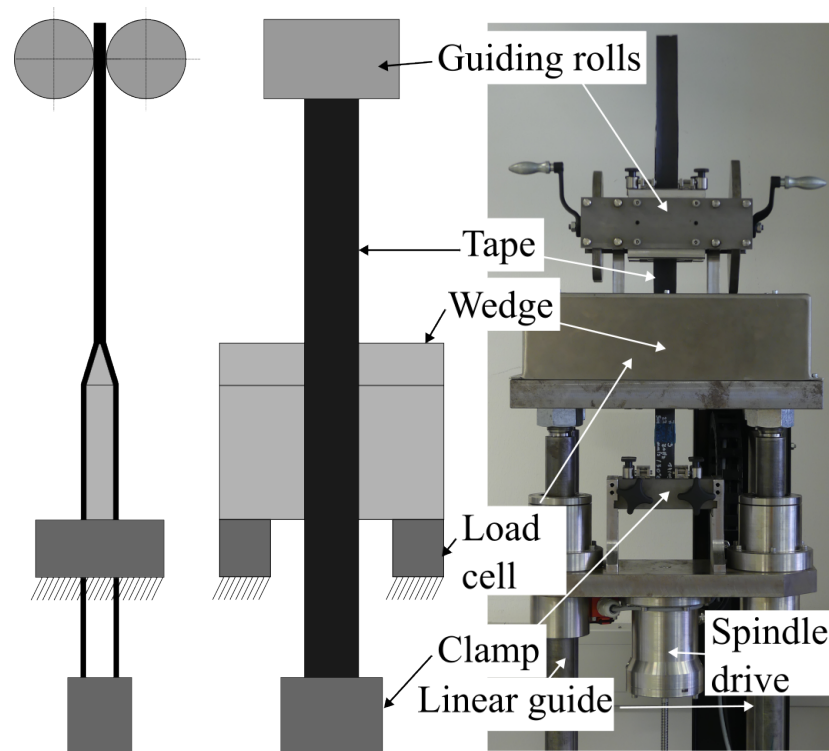


**Figure 2.** Side and front view of the wedge peel strength measuring rig used in this study.

In order to investigate the influence of humidity, the moisture of the tapes was measured before placement and before the wedge peel test. The moisture is measured using a Kern DAB 100-3 moisture analyzer. The moisture analyzer measures mass reduction with an accuracy of 0.003 g and a reproducibility of 0.15%.

### 2.5. Thermogravimetric Analysis

Thermogravimetric analysis was used to determine the degradation onset of the PA6 used for this study. The measurements were performed with a Mettler Toledo TGA/DSC 3+ STARE system. Samples were taken from random places and different positions along the length of multiple tapes in order to avoid systematic influences on the results. The weight of the samples ranged from 7 to 12 mg. The samples were heated from 25 °C up to 650 °C at a heating rate of 10 °C/min under a nitrogen atmosphere with a nitrogen flow of 50 mL/min.

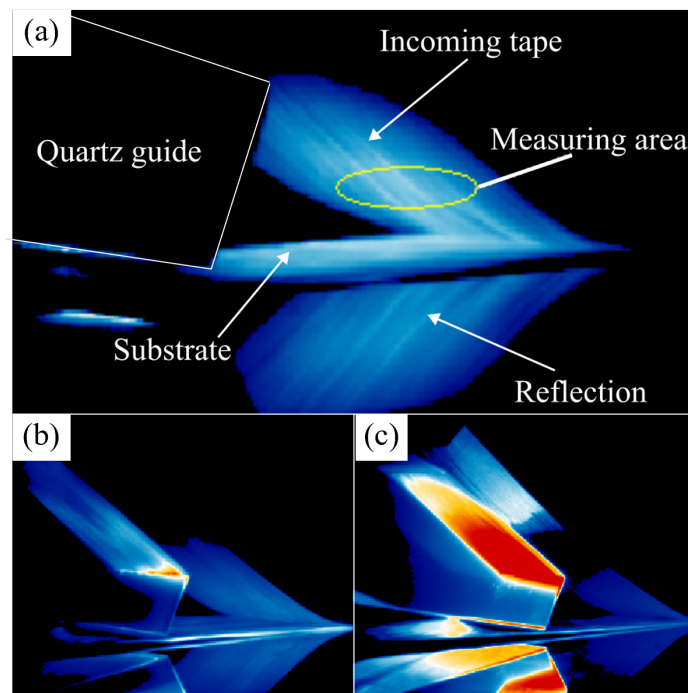
### 2.6. Differential Scanning Calorimetry

In order to measure the melting point and crystallization temperature of the material used for this study, DSC measurements were conducted. These measurements were used to link potential changes in peel strength to a change in molecular structure (e.g., melting and crystallization temperature). The DSC tests for this study were run on a Mettler Toledo DSC 1 device. The samples were heated from 30 °C to 280 °C (above the infinite polymer melting temperature of 270 °C [16]) with a heating rate of 10 °C/min and held at 280 °C for 5 min to erase the process history and remaining crystal seeds. After holding the samples at 280 °C, they were cooled to 30 °C at a cooling rate of 10 °C/min and then heated up to 280 °C at 10 °C/min again to evaluate any changes in the molecular structure due to degradation. All tests were performed under nitrogen atmosphere.

### 3. Results and Discussion

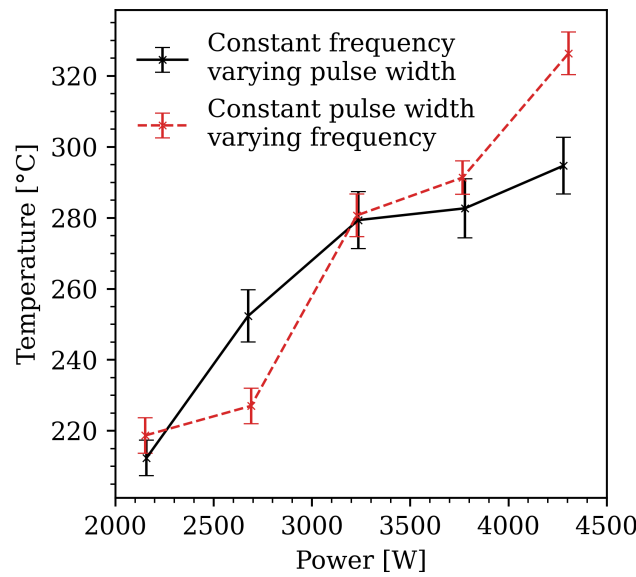
#### 3.1. Temperature Evaluation

Figure 3a shows the third layer of a tape placed at 50 mm/s onto two other tapes forming a  $[0]_4$  substrate. The evaluation area for the temperature measurement is shown with a yellow ellipse. All data were collected with an acquisition frequency of 250 Hz. An uneven heat distribution across the tape width can be seen in the Figure, as well as an uneven heat distribution along the tape length. Figure 3b,c show thermographs with a chamfered quartz guide, as shown in Figure 1b. It can be observed that the matrix residue of the tape was collecting on the chamfered sides of the quartz guide due to the tape touching the quartz guide during the end phase of the placement. This led to different heating characteristics in the subsequent tapes. The chamfered quartz guides led to a high variability in temperature over the tape length with increasing amounts of residue buildup. Figure 3c shows the quartz guide heating up to over 400 °C, which led to a heating of the tape right after exiting the guiding system and a lower temperature in front of the nip point compared to Figure 3b. The geometries with chamfered sides were found to be more sensitive to residue buildup on the quartz guides. The geometry in Figure 1a was therefore been chosen for all further experiments.



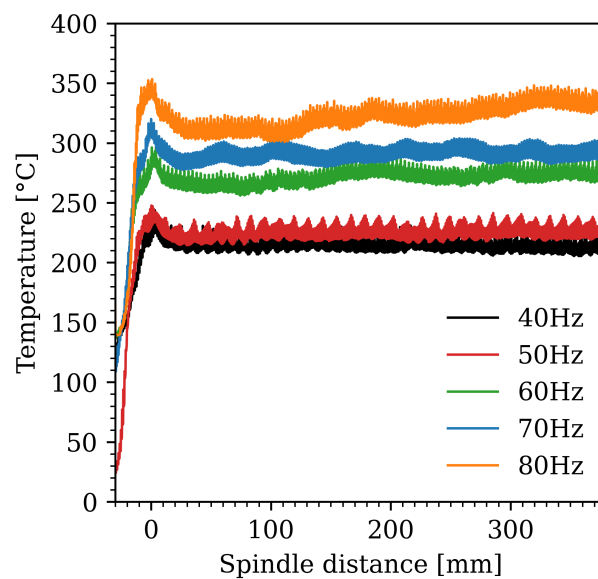
**Figure 3.** (a) Evaluation area for the temperature measurement. (b) Chamfered quartz guide after placing 3 tapes with 70 Hz and a pulse width of 1700  $\mu$ s. (c) Chamfered quartz guide after placing 11 tapes with heating of the quartz guide due to residue collection on the surface.

Figure 4 shows the temperature evolution for the different power settings. Each entry in the plot was derived from temperature measurements on three different tapes. The temperature was measured at uniform locations along the tape length in sections where samples for subsequent wedge peel tests were extracted. It can be seen that the constant frequency with varying pulse width samples experienced higher temperature with higher power compared to the constant pulse width samples, except for 2691 W (50 Hz). This could be explained by the frequency shift, which leads to a higher energy, as the energy of a photon is directly proportional to the wavelength. Furthermore, the higher frequency leads to a slight change in the spectrum emitted by the quartz guide. This different spectrum could lead to a change in heat transfer within the tape.



**Figure 4.** Process temperature for all power settings used in this study for constant frequency with varying pulse width (solid curve) and constant pulse width and varying frequency (dashed curve).

Figure 5 shows the temperature evolution over the tape length section relevant for the subsequent wedge peel tests for the tapes placed at a constant pulse width with varying frequency for one tape each. The spindle position 0 mm was at the beginning of the bonding between the tapes shortly after the start of the placement when the temperature reached a temperature level high enough to bond the tapes together. It can be seen that the temperatures for the experiments at 40 Hz and 50 Hz were closer to each other compared to the other values. The first peak in the temperature can be explained by the startup of the placement with the tape being closer to the quartz guide and therefore having a higher temperature. The temperature evolution for the experiments at 60 to 80 Hz showed higher variability within the peel test length. The 80 Hz sample showed the highest variability and increasing temperature over the peel test length, which could lead to different bonding within the tape over the length of the placement.



**Figure 5.** Temperature evolution over the wedge peel strength measuring distance for the tapes placed at constant pulse width with varying frequency.

### 3.2. Peel Strength

Figure 6 shows the results of the wedge peel strength tests and the tape width used for normalizing the peel strength data. The tape width after consolidation was measured at uniform locations for each tape with a caliber at 10 positions. The average of these measurements was used to calculate the wedge peel strength in the gray section seen in Figure 7. The temperature evaluation was also done with the temperature values in the gray section. The tape width after consolidation measured for the third layer was smaller compared to the first two layers. Those two layers experienced more heating and consolidation cycles and were therefore wider due to no squeeze flow restriction on the edges (e.g., adjacent tapes). The evaluation section differed for each peel test and was determined by a steady state section within the peel strength by using a moving average on the data. No other data cleaning was necessary, as no outliers could be found in the steady state section for the evaluation.

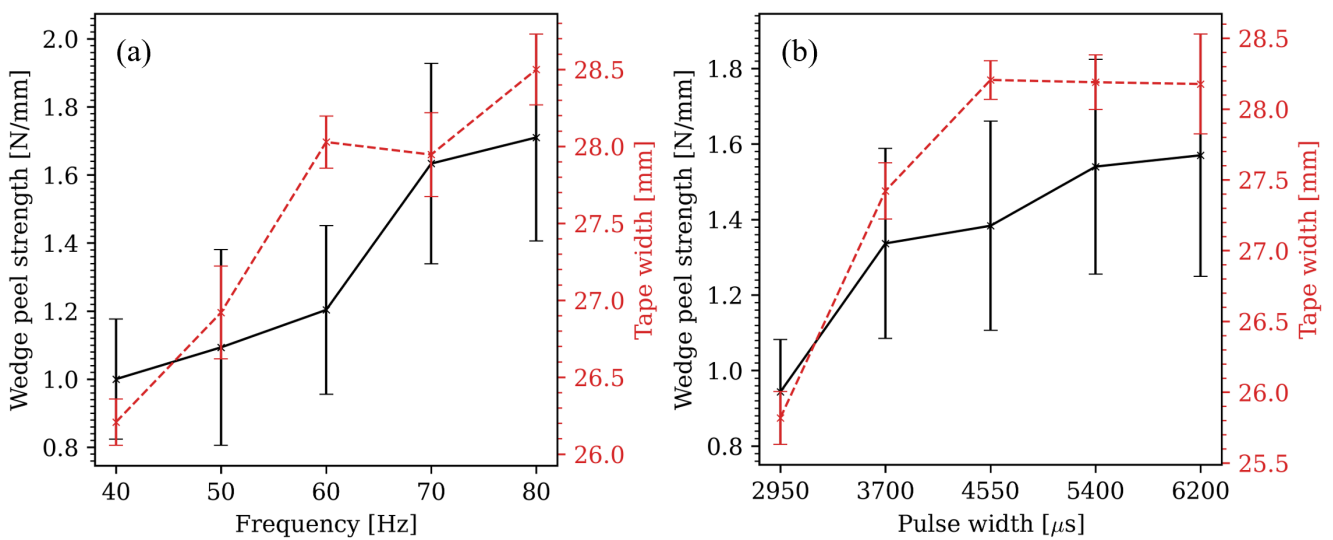


**Figure 6.** (a) Effects of the frequency on the wedge peels strength and the tape width. (b) Effects of the pulse width on the wedge peels strength and the tape width.

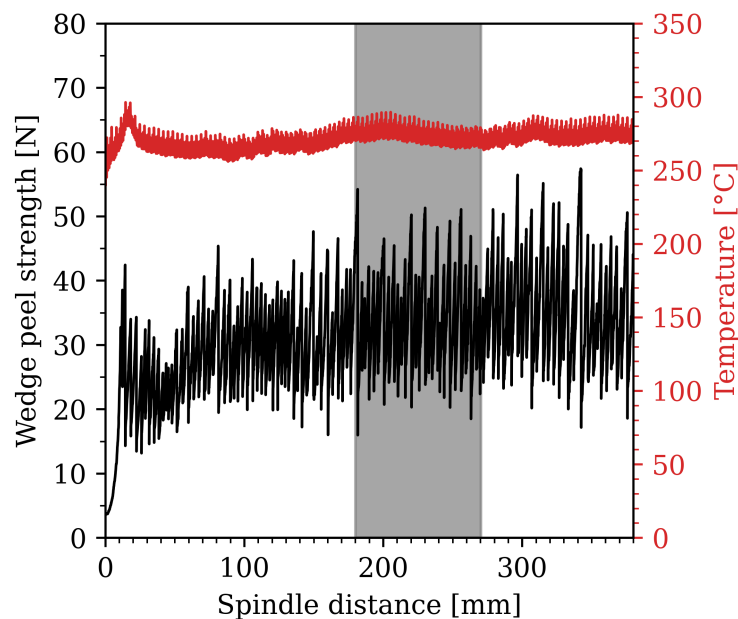


**Figure 7.** Peel strength and temperature over the peel test length for the 60 Hz sample.

All tapes were placed directly after they were taken out of the oven. The moisture was measured before the placement on 53 tapes. The tapes were dried in the moisture analyzer for 7 min at 120 °C. The average moisture was 1.61 m% with a standard deviation of 0.23 m%. This resulted in an about 1 m% lower moisture content compared to the samples before drying. The results for a constant pulse width (2200  $\mu$ s) and varying frequency can be seen in Figure 6a. A constant rise in peel strength with increasing frequency and therefore increasing power can be observed. The power is a function of the frequency, pulse width, and voltage of the setting. An increase in any of those three settings will lead to a higher power and therefore temperature (if all of the other process variables stay the same). The increase in temperature led to a higher bonding strength up to the point where matrix degradation took place or significant matrix squeeze out occurred due to the decrease in matrix viscosity. The lowest value (1.00 N/mm) was at 40 Hz (2153 W with 219 °C process temperature). The highest peel strength value (1.71 N/mm) was achieved with a frequency of 80 Hz and a temperature of 326 °C. However, the variation within the peel strength rose with increasing frequency and, thus, with temperature. Figure 6b shows the results from tests with constant frequency (30 Hz) and varying pulse width. The lowest value (0.94 N/mm) is at 2950  $\mu$ s (temperature of 212 °C) and the highest value (1.57 N/mm) can be found at 6200  $\mu$ s with a temperature of 295 °C. The variation within the peel strength increased with pulse width and, thus, again with temperature. In general, the peel strength values found in this study were lower than those reported by Stokes-Griffin et al. [16] for the same material. This could be explained by the lower lay-up speed used in this study (50 mm/s compared to 100 mm/s). This could lead to a higher degree of more ductile  $\gamma$  phases in the tapes placed at 100 mm/s, due to faster cooling. This increases the wedge peel strength. Furthermore the consolidation force was set to 500 N for 25.4 mm wide tapes in this study, whereas Stokes-Griffin et al. [16] used 130 N for 12 mm wide tapes. An analysis of the pressure distribution for the roller used in this study at 500 N showed that an average pressure of 1.57 MPa was applied to the tapes over the area of contact with the roller. The pressure was measured with a Prescale LLW pressure measuring film at a room temperature of 22.8 °C and a humidity of 26.8%. However, the resulting pressure and consolidation tape width were not known for the reference study. There, the highest wedge peel strength was reported with 4.3 N/mm at a process temperature of 260 °C. In general, a higher contact area is favorable to develop higher degrees of intimate contact; this, however, limits the pressure on the tapes, which in turn has negative consequences on the intimate contact [23].

In order to investigate the influence of humidity on the wedge peel strength, three samples for each of the drying conditions were prepared (Table 2).

**Table 2.** Drying conditions for investigating the moisture influence on the wedge peel strength (ND: nondried, D: dried).

Label	Drying before Placement	Drying before Peel-Test
ND/ND	72 h at 21 °C and 41% humidity	72 h at 21 °C and 41% humidity
ND/D	72 h at 21 °C and 41% humidity	72 h at 60 °C in vacuum oven
D/ND	48 h at 100 °C in vacuum oven	72 h at 21 °C and 41% humidity
D/D	48 h at 100 °C in vacuum oven	72 h at 60 °C in vacuum oven

The results can be seen in Figure 8. The ND/ND samples had the highest peel strength (2.04 N/mm), whereas the samples dried before the placement showed a significant reduction in peel strength resulting in a peel strength of around 0.9 N/mm. This is to be expected, because moisture acts as a plasticizer in the polymer. Plasticizers decrease

the  $T_g$  and  $T_m$  and provide chain mobility by reducing the secondary forces between the macromolecules. This effect results in a decrease in tensile strength, hardness, or elastic modulus while increasing the elongation at break or toughness [61]. Those effects result in a more ductile crack propagation compared to dry samples [62]. Samples not dried before the placement but dried before the peel test also showed a reduction in peel strength, but it was not as drastic compared to the samples dried before the placement. The peel strength for those samples reached an average level of 1.39 N/mm.

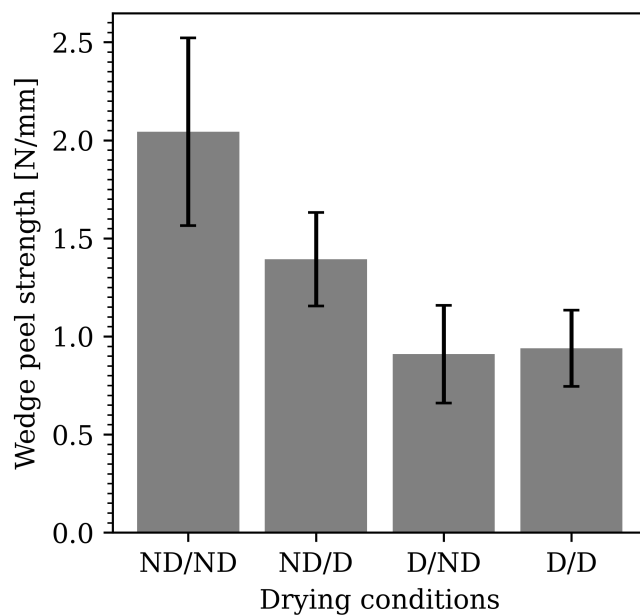


**Figure 8.** Effect of drying the samples before the placement and before the peel test on the wedge peel strength (ND: nondried, D: dried).

### 3.3. TGA Measurements

Thermal degradation deteriorates the polymer matrix by cutting the molecular chains by rupture or scission [63]. During ATP, heating rates of 500 °C/s can occur. However, the exposure to high temperature levels is usually very short (<0.2 s) [4,16]. Figure 9 shows the results from TGA tests on five composite material samples. The onset of degradation was annotated at around 362 °C and was set at a weight loss of 3%, because PA6 absorbs around 3 m% of water at standard conditions (23 °C and 50% humidity) [64]. These results were verified by measuring 17 tapes with the moisture analyzer. The tapes have been kept at a humidity of 43% and a temperature of 22 °C. All tapes were dried for 7 min at a temperature of 120 °C with the halogen lamp of the moisture analyzer. The tapes lost 2.73 m% water on average with a standard deviation of 0.11 m%. The degradation temperature for PA6 was found by other researchers at around 350 °C [65] to 400 °C [66], and the material was fully decomposed at around 500 °C [67] to 530 °C [66] in a nitrogen atmosphere. A temperature above 390 °C was shown to lead to a more intense degradation (the degradation took place faster) [68]. The water loss took place from the start of the measurements (25 °C) to the degradation point. A faster mass loss was seen from the start to around 150 °C. After this point to the degradation point, a slower loss was observed (around 1% mass loss from 150 °C to 360 °C). The degradation temperature was determined after the loss of all water (around 3 m%). This yielded a degradation temperature of 361.8 °C with a standard deviation of 8.6 °C. After the initial mass loss due to the absorbed water, the matrix degraded from 361.8 °C to around 500 °C, thus leaving around 56.3 m% (standard deviation of 0.5 m%) carbon fibers behind (at a temperature of 550 °C). The fiber mass content was 2.3 m% higher compared to the data sheet of the material. Slight deviations in the degradation temperature between the samples were observed. The fastest degradation

was found at 455.8 °C with a standard deviation of 1.0 °C. The results from Hanna [69] verify the decomposition stages found in this study: At temperature levels up to 150 °C, the matrix was losing absorbed water, which resulted in a small weight loss of about 2%. The second stage ranged from 280 to 450 °C, where the PA6 was getting decomposed, and above 450 °C, were the impurities and undecomposed PA6 were lost. A higher degree of crystallinity was found to lead to faster decomposition at higher temperature. A higher activation energy is needed at higher crystallinity to break the crystalline parts [69].

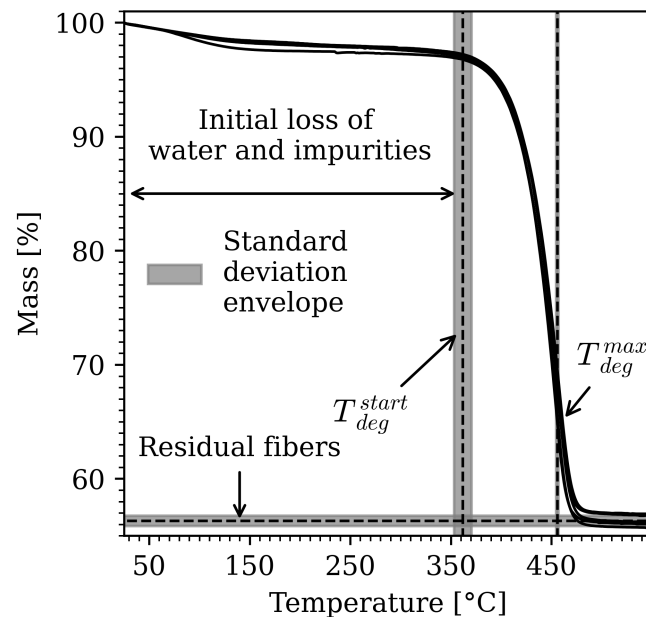


**Figure 9.** TGA curves of 5 samples with degradation onset annotated at 350 °C.

### 3.4. DSC Measurements

Figure 10a shows the two heating cycles and the cooling cycle for the sample placed at a frequency of 80 Hz and a pulse width of 2200  $\mu$ s. The heating cycle 1 was offset by 0.4 W/g for better visualization. The curves would otherwise fall together with the heating cycle 2. Both the melting and crystallization temperature were taken from the endothermic and exothermic peaks. It can be seen that the melting temperature of the as-processed samples (heating cycle 1) was around 2 °C higher compared to the heating cycle after cycling to the infinite polymer melting point  $T_m^\infty$ . This can also be seen for all other tested samples in Figure 10b, which showed samples ranging from 40 to 80 Hz and a sample at 30 Hz, which showed no bonding. A higher melting point was associated with the  $\alpha$  phase crystals, whereas a lower melting point was associated with the  $\gamma$  phase crystals. However, the  $\alpha$  phase formed at slow cooling rates, and the  $\gamma$  phase at fast cooling rates.  $\alpha$  phase crystals have a melting temperature of around 225 °C and the  $\gamma$  phase crystals at 215 °C [63]. The heating and cooling rates of the ATP process, however, were much higher compared to the 10 °C/min used in the DSC. Therefore, the samples manufactured by ATP would have a higher degree of the  $\gamma$  phase. The formation of the crystalline structure is influenced by thermal conditions, applied stress, additives within the polymer [70], water content [71], or high pressure during crystallization [72]. The  $\alpha$  phase is observed to form at temperatures above 190 °C, and the  $\gamma$  phase below 130 °C when the polymer is kept at those temperatures for longer periods of time. At temperature levels between 130 °C and 190 °C, a mixture of both phases will be present. Short crystallization times at 200 °C can lead to both crystallization forms [73]. The results from Figure 10a indicate that there was a higher amount of  $\alpha$  phase crystals in the first heating cycle resulting in a higher melting temperature. The endothermic heat flow was more narrow compared to the heat flow of the second heating cycle, thus indicating the  $\alpha$  phase [74]. A wide

heat flow curve indicates either the  $\gamma$  phase or the  $\beta$  phase (also called mesophase). The mesophase, however, was a result of high cooling rates of thin samples and not likely to occur at 10 °C/min cooling rates [75,76]. Both the  $\gamma$  and  $\beta$  phase are hard to distinguish using DSC. Wide-angle X-ray scattering is a method commonly used to distinguish between the different crystalline phases. However, the  $\gamma$  and  $\beta$  phase share a similar scattering angle [74,76]. A clear description of the crystalline phase is not possible with DSC tests. Changes in the crystallinity can also occur during the heating cycle of the DSC tests. The evaluation of the crystalline phase of the processing parameters used in this work needs to be investigated in a future study. The  $T_g$  could not be determined in the samples. This is possibly due the moisture in the sample. Studies have found that the time of sample preparation is sufficient to absorb enough moisture for the  $T_g$  to drop from the dry value of around 54 °C to a value between 15 °C and 20 °C. Due to the starting point of the DSC in this test (25 °C), the  $T_g$  did not appear in the samples. Furthermore, the  $T_g$  is likely to be overseen in undried samples, as the moisture loss during the DSC would overlap with the silent exothermic crystallization [77].

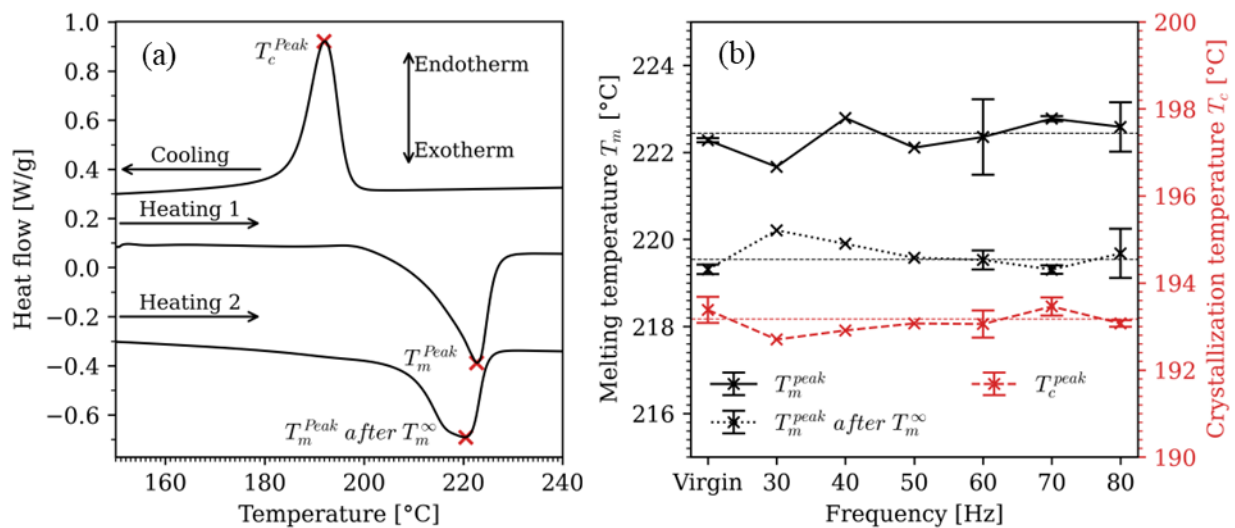


**Figure 10.** (a) DSC heating and cooling cycles for different heating system frequencies (Heating cycle 1 offset by 0.4 W/g for better visualization). (b) Melting temperature before and after cycling to the melting point of the infinite crystals, as well as crystallization temperature (all temperatures are peak values).

### 3.5. Micrographs

Figure 11 shows cross-sections of polished samples from different heating system parameter variations (corresponding to the values in Table 1) around 300 mm from the start of the lay-up. The cross-sections were used to evaluate the homogeneity of the laminates and not to analyze any damages resulting from the placement. All images were taken with a digital microscope from Keyence (VHX-7000) at a magnification of 150×. At the lower power levels (to around 3229 W) of the tapes with constant pulse width, the individual tapes of each layer can be clearly distinguished, whereas the layers of the tapes with constant frequency cannot be clearly separated from 2676 W upwards. This corresponds to the peel strength values shown in Figure 6. The clearly separable samples show lower wedge peel strength (<1.3 N/mm). At higher wedge peel strengths, the different states of inhomogeneity of the tape became less visible. The thickness of the samples was measured with ImageJ over 25 points across the tape width. The thickness of the tapes with a constant pulse width showed a linear trend of decreasing thickness with increasing frequency. The tape with 40 Hz had a average thickness of 0.796 mm with a standard deviation of 0.011 mm, whereas the tape placed with 80 Hz had a thickness of 0.651 mm with a standard deviation of 0.015 mm. The thickness of the tapes placed with constant

frequency showed more variation and no linear trend. The tape placed with 2950  $\mu\text{s}$  had a thickness of 0.765 mm and a standard deviation of 0.013 mm, whereas the tape placed with 6200  $\mu\text{s}$  had a thickness of 0.675 mm and a standard deviation of 0.025 mm. A full overview of the measured tape thickness is shown in Table 3. The reduction in thickness is attributed to the higher processing temperature and matrix squeeze-out due to lower matrix viscosity at elevated temperature. The fluctuation of the thickness with increasing temperature can be explained with uneven tape thickness and varying temperature during the placement due to the pulsing operation of the system and nonuniform fiber volume fraction along the tape. Another possible explanation for the varying thickness reduction in the samples with constant frequency could be due to a higher matrix viscosity compared to the samples with varying frequency. Higher frequencies could lead to a higher excitement of the molecular chains and thus reducing the London dispersion forces, which reduces the matrix viscosity [78]. Moreover, a shift in frequency could also lead to a shift in wavelength, which could result in a better absorption of the energy emitted from the light source by the molecules.

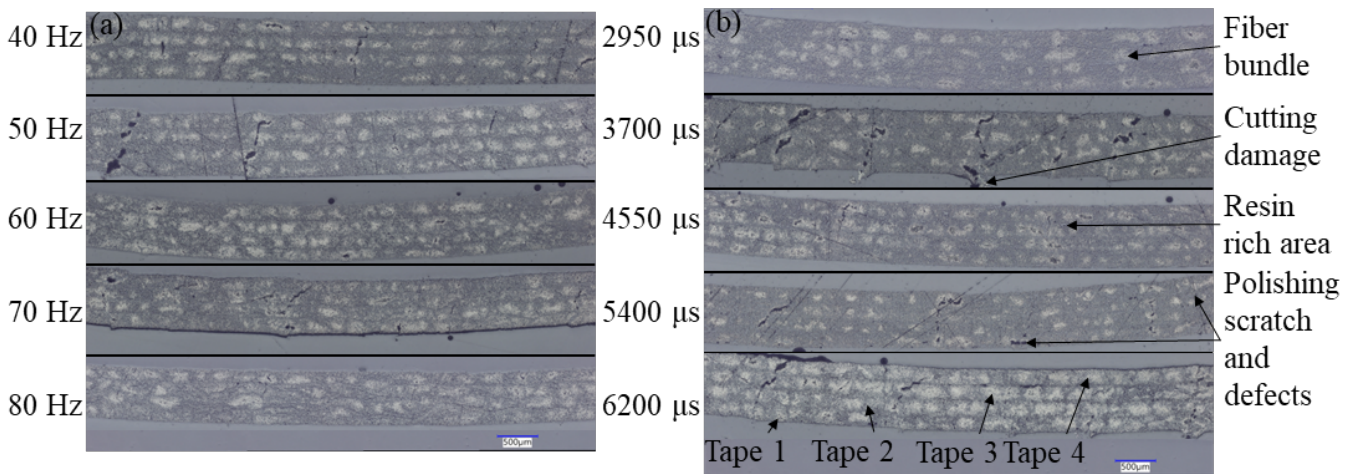


**Figure 11.** Micrographs of the center of the samples from different heating system parameters. (a) Frequencies from 40 Hz to 80 Hz and constant pulse width of 2200  $\mu\text{s}$ . (b) Pulse widths from 2950  $\mu\text{s}$  to 6200  $\mu\text{s}$  and constant frequency of 30 Hz.

**Table 3.** Tape thickness measured from micrographs for all processing conditions.

Frequency [Hz]	Pulse Width [ $\mu\text{s}$ ]	Mean Thickness [mm]	Standard Deviation [mm]
40	2200	0.796	0.011
50	2200	0.767	0.012
60	2200	0.685	0.010
70	2200	0.667	0.011
80	2200	0.651	0.015
30	2950	0.765	0.013
30	3700	0.729	0.012
30	4550	0.747	0.010
30	5400	0.756	0.014
30	6200	0.675	0.025

#### 4. Conclusions

In this study, the impact of the processing conditions of a flashlamp heating system on the bonding strength and the temperature evolution of the incoming tape was evaluated. Furthermore, the influence of moisture within the CF/PA6 tapes on the bonding strength was investigated. The bonding strength between the layers was investigated using a wedge

peel test rig. The frequency and the pulse width of the flashlamp heating system were varied, and their effects on 25.4 mm wide tapes placed at 50 mm/s were analyzed. TGA was used to determine the degradation temperature of the material used in this study. A degradation temperature of around 362 °C was found by analyzing five samples. DSC measurements of samples placed with different frequency settings and constant pulse width were analyzed, as well as micrographs for all parameter combinations. The DSC measurements showed no thermal degradation, which would lead to changes in the melting or crystallization temperature. The melting temperature was found to be around 222 °C right after processing and at 219 °C after cycling to the infinite melting point of the polymer. The crystallization temperature was found to be at around 193 °C. No significant differences could be seen for the tested samples. Micrographs showed a linear thickness reduction of the samples manufactured at a constant pulse width, whereas the thickness of the samples placed with constant frequency showed varying thickness with higher temperature. A decreasing thickness correlated with an increase in wedge peel strength. It has to be noted that a higher matrix squeeze out could lead to a significant loss in wedge peel strength. Matrix squeeze out reduced the resin rich areas between the tapes, which is expected to reduce the bonding strength [16]. More matrix squeeze out was to be expected at higher temperature. It was seen that a higher temperature led to higher residue buildup on the quartz guides used for the flashlamp system. Chamfered guides were more susceptible to residue buildup, as the tape drags over the chamfered radiating surfaces at the end of the lay-up. The quartz guide with only one radiating surface (directed at the nip-point) was seen to be more stable in terms of temperature as less residue was building up on this geometry. The humidity was found to be a significant factor regarding the bonding. Samples dried before placement had lower peel strength compared to nondried samples. This is the result of the plasticizing effect of moisture within the polymer matrix. The highest peel strength was found to be at a frequency of 80 Hz and a pulse width of 2200 µs. This sample furthermore showed the highest temperature. The variation in the wedge peel strength increased with higher temperature, as well as the variation within the temperature. The results for the DSC and TGA measurements in this study were expected. The increase in peel strength with power is to be expected; however, the differences between a higher frequency and a higher pulse width (while keeping the other parameter low) were not expected at identical power values. More research needs to be conducted to explain these results in more detail. An analysis of the emitted spectral range of the flashlamp system should be conducted to gain a deeper insight into the heat transfer of the heating system.

**Author Contributions:** Conceptualization, A.L.; methodology, A.L. and E.F.; validation, A.L.; formal analysis, A.L.; investigation, A.L.; resources, E.F.; data curation, A.L.; writing—original draft preparation, A.L.; writing—review and editing, E.F.; visualization, A.L.; supervision, E.F. All authors have read and agreed to the published version of the manuscript.

**Funding:** This research received no external funding.

**Data Availability Statement:** The data presented in this study are available upon reasonable request from the corresponding author.

**Acknowledgments:** Technical support from the Chair of Materials Science and Testing of Polymers and the Chair of Chemistry of Polymeric Materials, Montanuniversität Leoben, is kindly acknowledged.

**Conflicts of Interest:** The authors declare no conflicts of interest.

## References

1. Neitzel, M.; Mitschang, P.; Breuer, U. (Eds.) *Handbuch Verbundwerkstoffe: Werkstoffe, Verarbeitung, Anwendung*; Carl Hanser Verlag GmbH Co KG: München, Germany, 2014.
2. Schledjewski, R. Thermoplastic tape placement process—In situ consolidation is reachable. *Plast. Rubber Compos.* **2009**, *38*, 379–386. [[CrossRef](#)]
3. Lukaszewicz, D.H.J.; Ward, C.; Potter, K.D. The engineering aspects of automated prepreg layup: History, present and future. *Compos. Part B Eng.* **2012**, *43*, 997–1009. [[CrossRef](#)]

4. Stokes-Griffin, C.M.; Compston, P. The effect of processing temperature and placement rate on the short beam strength of carbon fibre-PEEK manufactured using a laser tape placement process. *Compos. Part A Appl. Sci. Manuf.* **2015**, *78*, 274–283. [[CrossRef](#)]
5. Jiang, W.; Chen, C.; Chen, Z.; Huang, Z.; Zhou, H. Effect of crystallinity on optical properties of PEEK prepreg tapes for laser-assisted automated fiber placement. *Compos. Commun.* **2023**, *38*, 101490. [[CrossRef](#)]
6. Shafaq; Donough, M.J.; Farnsworth, A.L.; Phillips, A.W.; St John, N.A.; Gangadhara Prusty, B. Influence of deposition rates on the mode I fracture toughness of in-situ consolidated thermoplastic composites. *Compos. Part B Eng.* **2023**, *251*, 110474. [[CrossRef](#)]
7. Khodaei, A.; Shadmehri, F. Intimate contact development for automated fiber placement of thermoplastic composites. *Compos. Part C Open Access* **2022**, *8*, 100290. [[CrossRef](#)]
8. Zhang, C.; Duan, Y.; Xiao, H.; Wang, B.; Ming, Y.; Zhu, Y.; Zhang, F. Effect of porosity and crystallinity on mechanical properties of laser in-situ consolidation thermoplastic composites. *Polymer* **2022**, *242*, 124573. [[CrossRef](#)]
9. Oromiehie, E.; Prusty, B.G.; Compston, P.; Rajan, G. Automated fibre placement based composite structures: Review on the defects, impacts and inspections techniques. *Compos. Struct.* **2019**, *224*, 110987. [[CrossRef](#)]
10. Çelik, O.; Bussink, T.; Peeters, D.; Teuwen, J.; Dransfeld, C. The effect of Laser-Induced deconsolidation on the compaction behavior of thermoplastic composite tapes. *Compos. Part A Appl. Sci. Manuf.* **2021**, *151*, 106670. [[CrossRef](#)]
11. Miao, Q.; Dai, Z.; Ma, G.; Niu, F.; Wu, D. Effect of consolidation force on interlaminar shear strength of CF/PEEK laminates manufactured by laser-assisted forming. *Compos. Struct.* **2021**, *266*, 113779. [[CrossRef](#)]
12. Chanteli, A.; Bandaru, A.K.; Peeters, D.; O'Higgins, R.M.; Weaver, P.M. Influence of repress treatment on carbon fibre-reinforced PEEK composites manufactured using laser-assisted automatic tape placement. *Compos. Struct.* **2020**, *248*, 112539. [[CrossRef](#)]
13. Clancy, G.; Peeters, D.; Oliveri, V.; Jones, D.; O'Higgins, R.M.; Weaver, P.M. A study of the influence of processing parameters on steering of carbon Fibre/PEEK tapes using laser-assisted tape placement. *Compos. Part B Eng.* **2019**, *163*, 243–251. [[CrossRef](#)]
14. Martín, M.I.; Rodríguez-Lence, F.; Güemes, A.; Fernández-López, A.; Pérez-Maqueda, L.A.; Perejón, A. On the determination of thermal degradation effects and detection techniques for thermoplastic composites obtained by automatic lamination. *Compos. Part A Appl. Sci. Manuf.* **2018**, *111*, 23–32. [[CrossRef](#)]
15. Slange, T.K.; Warnet, L.L.; Groupe, W.; Akkerman, R. Deconsolidation of C/PEEK blanks: On the role of prepreg, blank manufacturing method and conditioning. *Compos. Part A Appl. Sci. Manuf.* **2018**, *113*, 189–199. [[CrossRef](#)]
16. Stokes-Griffin, C.M.; Kollmannsberger, A.; Compston, P.; Drechsler, K. The effect of processing temperature on wedge peel strength of CF/PA 6 laminates manufactured in a laser tape placement process. *Compos. Part A Appl. Sci. Manuf.* **2019**, *121*, 84–91. [[CrossRef](#)]
17. Stokes-Griffin, C.M.; Compston, P. An inverse model for optimisation of laser heat flux distributions in an automated laser tape placement process for carbon-fibre/PEEK. *Compos. Part A Appl. Sci. Manuf.* **2016**, *88*, 190–197. [[CrossRef](#)]
18. Comer, A.J.; Ray, D.; Obande, W.O.; Jones, D.; Lyons, J.; Rosca, I.; O' Higgins, R.M.; McCarthy, M.A. Mechanical characterisation of carbon fibre-PEEK manufactured by laser-assisted automated-tape-placement and autoclave. *Compos. Part A Appl. Sci. Manuf.* **2015**, *69*, 10–20. [[CrossRef](#)]
19. Stokes-Griffin, C.M.; Compston, P. Optical characterisation and modelling for oblique near-infrared laser heating of carbon fibre reinforced thermoplastic composites. *Opt. Lasers Eng.* **2015**, *72*, 1–11. [[CrossRef](#)]
20. Khan, M.A.; Mitschang, P.; Schledjewski, R. Parametric study on processing parameters and resulting part quality through thermoplastic tape placement process. *J. Compos. Mater.* **2013**, *47*, 485–499. [[CrossRef](#)]
21. Pérez-Martín, H.; Buchalik-Bopp, S.; Guettler, B.E.; Mackenzie, P.; Baidak, A.; Ó Brádaigh, C.M.; Ray, D. Effect of crystallinity and morphology on the mechanical properties of CF/PEEK composites manufactured under compression moulding and automated tape placement. *Mater. Today Commun.* **2023**, *36*, 106442. [[CrossRef](#)]
22. Fuessel, L.; Cender, T.A.; Austermann, V.; Gillespie, J.W., Jr.; Heider, D. Tow Steering of stretchable TuFF thermoplastic tape with laser tape placement. In Proceedings of the SAMPE 2022—Charlotte, NC, Proceedings, Charlotte, NC, USA, 23–26 May 2022; pp. 700–711.
23. Çelik, O.; Peeters, D.; Dransfeld, C.; Teuwen, J. Intimate contact development during laser assisted fiber placement: Microstructure and effect of process parameters. *Compos. Part A Appl. Sci. Manuf.* **2020**, *134*, 105888. [[CrossRef](#)]
24. Chen, J.; Fu, K.; Li, Y. Understanding processing parameter effects for carbon fibre reinforced thermoplastic composites manufactured by laser-assisted automated fibre placement (AFP). *Compos. Part A Appl. Sci. Manuf.* **2021**, *140*, 106160. [[CrossRef](#)]
25. Chadwick, A.R.; Kotzur, K.; Nowotny, S. Moderation of thermoplastic composite crystallinity and mechanical properties through in situ manufacturing and post-manufacturing tempering: Part 1 – Mechanical characterisation. *Compos. Part A Appl. Sci. Manuf.* **2021**, *143*, 106286. [[CrossRef](#)]
26. Groupe, W.J.B.; Vanden Poel, G.; Warnet, L.L.; Akkerman, R. On crystallisation and fracture toughness of poly(phenylene sulphide) under tape placement conditions. *Plast. Rubber Compos.* **2013**, *42*, 282–288. [[CrossRef](#)]
27. Groupe, W.; Warnet, L.L.; Rietman, B.; Akkerman, R. On the weld strength of in situ tape placed reinforcements on weave reinforced structures. *Compos. Part A Appl. Sci. Manuf.* **2012**, *43*, 1530–1536. [[CrossRef](#)]
28. Stokes-Griffin, C.M.; Kollmannsberger, A.; Ehard, S.; Compston, P.; Drechsler, K. Manufacture of steel-CF/PA6 hybrids in a laser tape placement process: Effect of first-ply placement rate on thermal history and lap shear strength. *Compos. Part A Appl. Sci. Manuf.* **2018**, *111*, 42–53. [[CrossRef](#)]
29. Schaefer, P.M.; Guglhoer, T.; Sause, M.G.; Drechsler, K. Development of intimate contact during processing of carbon fiber reinforced Polyamide-6 tapes. *J. Reinf. Plast. Compos.* **2017**, *36*, 593–607. [[CrossRef](#)]

30. Schaefer, P.M.; Gierszewski, D.; Kollmannsberger, A.; Zaremba, S.; Drechsler, K. Analysis and improved process response prediction of laser-assisted automated tape placement with PA-6/carbon tapes using Design of Experiments and numerical simulations. *Compos. Part A Appl. Sci. Manuf.* **2017**, *96*, 137–146. [[CrossRef](#)]
31. Kukla, C.; Peters, T.; Janssen, H.; Brecher, C. Joining of Thermoplastic Tapes with Metal Alloys Utilizing Novel Laser Sources and Enhanced Process Control in a Tape Placement Process. *Procedia CIRP* **2017**, *66*, 85–90. [[CrossRef](#)]
32. Steyer, M. Laserunterstütztes Tapelegeverfahren zur Fertigung Endlosfaserverstärkter Thermoplastlaminat. Ph.D. Thesis, RWTH Aachen, Aachen, Germany, 2013.
33. Brecher, C.; Dubratz, M.; Stimpfl, J.; Emonts, M. Innovative manufacturing of 3D-lightweight components. *Laser Tech. J.* **2011**, *8*, 36–40. [[CrossRef](#)]
34. Chu, Q.; Li, Y.; Xiao, J.; Huan, D.; Zhang, X.; Chen, X. Processing and characterization of the thermoplastic composites manufactured by ultrasonic vibration-assisted automated fiber placement. *J. Thermoplast. Compos. Mater.* **2018**, *31*, 339–358. [[CrossRef](#)]
35. Rizzolo, R.H.; Walczyk, D.F. Ultrasonic consolidation of thermoplastic composite prepreg for automated fiber placement. *J. Thermoplast. Compos. Mater.* **2016**, *29*, 1480–1497. [[CrossRef](#)]
36. Baley, C.; Kervoëlen, A.; Lan, M.; Cartié, D.; Le Duigou, A.; Bourmaud, A.; Davies, P. Flax/PP manufacture by automated fibre placement (AFP). *Mater. Design* **2016**, *94*, 207–213. [[CrossRef](#)]
37. Brecher, C.; Emonts, M.; Schares, R.L.; Stimpfl, J. CO<sub>2</sub>-laser-assisted processing of glass fiber-reinforced thermoplastic composites. In Proceedings of the High-Power Laser Materials Processing: Lasers, Beam Delivery, Diagnostics, and Applications II; SPIE Processings, San Francisco, CA, USA, 22 February 2013; pp. 144–154. [[CrossRef](#)]
38. Wazeer, A.; Das, A.; Abeykoon, C.; Sinha, A.; Karmakar, A. Composites for electric vehicles and automotive sector: A review. *Green Energy Intell. Transp.* **2023**, *2*, 100043. [[CrossRef](#)]
39. Nishida, H.; Carvelli, V.; Fujii, T.; Okubo, K. Thermoplastic vs. thermoset epoxy carbon textile composites. *IOP Conf. Ser. Mater. Sci. Eng.* **2018**, *406*, 012043. [[CrossRef](#)]
40. Moghadamzad, M.; Hoa, S.V. Models for heat transfer in thermoplastic composites made by automated fiber placement using hot gas torch. *Compos. Part C Open Access* **2022**, *7*, 100214. [[CrossRef](#)]
41. Gain, A.K.; Oromiehie, E.; Prusty, B.G. Nanomechanical characterisation of CF-PEEK composites manufactured using automated fibre placement (AFP). *Compos. Commun.* **2022**, *31*, 101109. [[CrossRef](#)]
42. Oromiehie, E.; Gain, A.K.; Donough, M.J.; Prusty, B.G. Fracture toughness assessment of CF-PEEK composites consolidated using hot gas torch assisted automated fibre placement. *Compos. Struct.* **2022**, *279*, 114762. [[CrossRef](#)]
43. Satheesh, B.; Tonejc, M.; Potakowskyj, L.; Pletz, M.; Fauster, E.; Kaynak, B.; Schledjewski, R. Peel strength characterisation on ply/ply interface using wedge and T-peel/pull-type tests. *Polym. Polym. Compos.* **2018**, *26*, 431–445. [[CrossRef](#)]
44. Rajasekaran, A.; Shadmehri, F. Steering of carbon fiber/PEEK tapes using Hot Gas Torch-assisted automated fiber placement. *J. Thermoplast. Compos. Mater.* **2022**, *36*, 1651–1679. [[CrossRef](#)]
45. Groupe, W. Weld Strength of Laser-Assisted Tape-Placed Thermoplastic Composites. Ph.D. Thesis, University of Twente, Enschede, The Netherlands, 2012.
46. Danezis, A.; Williams, D.; Edwards, M.; Skordos, A.A. Heat transfer modelling of flashlamp heating for automated tape placement of thermoplastic composites. *Compos. Part A Appl. Sci. Manuf.* **2021**, *145*, 106381. [[CrossRef](#)]
47. Di Boon, Y.; Joshi, S.C.; Bhudolia, S.K. Review: Filament Winding and Automated Fiber Placement with In Situ Consolidation for Fiber Reinforced Thermoplastic Polymer Composites. *Polymers* **2021**, *13*, 1951. [[CrossRef](#)]
48. Meister, S.; Kolbe, A.; Groves, R.M. Reflectivity and emissivity analysis of thermoplastic CFRP for optimising Xenon heating and thermographic measurements. *Compos. Part A Appl. Sci. Manuf.* **2022**, *158*, 106972. [[CrossRef](#)]
49. Brandt, L.; Deden, D.; Fischer, F.; Bruckner, F.; Dreher, P.; Williams, D.J.; Engelschall, M.; Nieberl, D.; Nowotny, S. Xenon flashlamp based in-situ automated fiber placement of thermoplastic composites. In Proceedings of the 2019 International Conference on Composite Materials (ICCM), Melbourne, Australia, 11–16 August 2019; pp. 1–8.
50. Monnot, P.; Williams, D.; Di Francesco, M. Power Control of a Flashlamp-based Heating Solution for Automated Dry Fibre Placement. In Proceedings of the Proceedings 18th European Conference on Composite Materials, Athens, Greece, 25–28 June 2018; pp. 1–8.
51. Kollmannsberger, A. Heating Characteristics of Fixed Ofcus Laser Assisted Thermoplastic-Automated Fiber Placement of 2D and 3D Parts. Ph.D. Thesis, Technische Universität München, Munich, Germany, 2019.
52. Dolo, G.; Férec, J.; Cartié, D.; Grohens, Y.; Ausias, G. Model for thermal degradation of carbon fiber filled poly(ether ether ketone). *Polym. Degrad. Stab.* **2017**, *143*, 20–25. [[CrossRef](#)]
53. Stokes-Griffin, C.M.; Compston, P. Investigation of sub-melt temperature bonding of carbon-fibre/PEEK in an automated laser tape placement process. *Compos. Part A Appl. Sci. Manuf.* **2016**, *84*, 17–25. [[CrossRef](#)]
54. Stokes-Griffin, C.M.; Compston, P. A combined optical-thermal model for near-infrared laser heating of thermoplastic composites in an automated tape placement process. *Compos. Part A Appl. Sci. Manuf.* **2015**, *75*, 104–115. [[CrossRef](#)]
55. Schledjewski, R. Mechanical performance of in-situ consolidated thermoplastic fiber reinforced tape materials. In Proceedings of the 11th European Conference on Composite Materials, Rhodes, Greece, 31 May–3 June 2004; ECCM, Ed.; pp. 1–8.
56. Wanigasekara, C.; Oromiehie, E.; Swain, A.; Prusty, B.G.; Nguang, S.K. Machine Learning Based Predictive Model for AFP-Based Unidirectional Composite Laminates. *IEEE Trans. Ind. Inform.* **2020**, *16*, 2315–2324. [[CrossRef](#)]

57. Qureshi, Z.; Swait, T.; Scaife, R.; El-Dessouky, H.M. In situ consolidation of thermoplastic prepreg tape using automated tape placement technology: Potential and possibilities. *Compos. Part B Eng.* **2014**, *66*, 255–267. [[CrossRef](#)]
58. Schäfer, P.M. Consolidation of Carbon Fiber Reinforced Polyamide 6 Tapes Using Laser-Assisted Tape Placement. Ph.D. Thesis, Technische Universität München, Munich, Germany, 2018.
59. Zhang, C.; Duan, Y.; Xiao, H.; Wang, B.; Ming, Y.; Zhu, Y.; Zhang, F. The effects of processing parameters on the wedge peel strength of CF/PEEK laminates manufactured using a laser tape placement process. *Int. J. Adv. Manuf. Technol.* **2022**, *120*, 7251–7262. [[CrossRef](#)]
60. Hulcher, B.; Marchello, J.M.; Hinkley, J.A. Correlation between double cantilever beam and wedge peel tests for automated tow placement. In Proceedings of the 43rd International SAMPE Symposium and Exhibition, Anaheim, CA, USA, 31 May–4 June 1998; SAMPE, Ed.; pp. 1955–1965.
61. Bonifacio, A.; Bonetti, L.; Piantanida, E.; de Nardo, L. Plasticizer design strategies enabling advanced applications of cellulose acetate. *Eur. Polym. J.* **2023**, *197*, 112360. [[CrossRef](#)]
62. Piao, H.; Chen, L.; Kiryu, Y.; Ohsawa, I.; Takahashi, J. Influence of Water Absorption and Temperature on the Mechanical Properties of Discontinuous Carbon Fiber Reinforced Polyamide 6. *Fibers Polym.* **2019**, *20*, 611–619. [[CrossRef](#)]
63. Liang, J.; Xu, Y.; Wei, Z.; Song, P.; Chen, G.; Zhang, W. Mechanical properties, crystallization and melting behaviors of carbon fiber-reinforced PA6 composites. *J. Therm. Anal. Calorim.* **2014**, *115*, 209–218. [[CrossRef](#)]
64. Thirumalai, D.P.R.; Andersen, T.L.; Lystrup, A. Influence of Moisture Absorption on Properties of Fiber Reinforced Polyamide 6 Composites. In Proceedings of the 26th Annual Technical Conference of the American Society for Composites 2011 and the 2nd Joint US-Canada Conference on Composites, Montreal, QC, Canada, 26–28 September 2011; Hyer, M., Ed.; pp. 500–510.
65. Levchik, S.V.; Weil, E.D.; Lewin, M. Thermal decomposition of aliphatic nylons. *Polym. Int.* **1999**, *48*, 532–557. [[CrossRef](#)]
66. An, H.J.; Kim, J.S.; Kim, K.Y.; Lim, D.Y.; Kim, D.H. Mechanical and thermal properties of long carbon fiber-reinforced polyamide 6 composites. *Fibers Polym.* **2014**, *15*, 2355–2359. [[CrossRef](#)]
67. Tranchard, P.; Duquesne, S.; Samyn, F.; Estèbe, B.; Bourbigot, S. Kinetic analysis of the thermal decomposition of a carbon fibre-reinforced epoxy resin laminate. *J. Anal. Appl. Pyrolysis* **2017**, *126*, 14–21. [[CrossRef](#)]
68. Luederwald, I.; Merz, F.; Rothe, M. Ueber den thermischen abbau des poly-e-caprolactams (Nylon-6). *Angew. Makromol. Chem.* **1978**, *67*, 193–202. [[CrossRef](#)]
69. Hanna, A.A. Thermal and dielectric properties of nylon 6. *Thermochim. Acta* **1984**, *76*, 97–103. [[CrossRef](#)]
70. Fornes, T.D.; Paul, D.R. Crystallization behavior of nylon 6 nanocomposites. *Polymer* **2003**, *44*, 3945–3961. [[CrossRef](#)]
71. Campoy, I.; Gómez, M.A.; Marco, C. Structure and thermal properties of blends of nylon 6 and a liquid crystal copolyester1 Dedicated to the memory of Prof. J.G. Fatou.1. *Polymer* **1998**, *39*, 6279–6288. [[CrossRef](#)]
72. Hiramatsu, N.; Hirakawa, S. Melting and Transformation Behavior of  $\gamma$  Form Nylon 6 under High Pressure. *Polym. J.* **1982**, *14*, 165–171. [[CrossRef](#)]
73. Kyotani, M.; Mitsuhashi, S. Studies on crystalline forms of nylon 6. II. Crystallization from the melt. *J. Polym. Sci. Part A-2 Polym. Phys.* **1972**, *10*, 1497–1508. [[CrossRef](#)]
74. Millot, C.; Fillot, L.A.; Lame, O.; Sotta, P.; Seguela, R. Assessment of polyamide-6 crystallinity by DSC. *J. Therm. Anal. Calorim.* **2015**, *122*, 307–314. [[CrossRef](#)]
75. Parodi, E.; Govaert, L.E.; Peters, G. Glass transition temperature versus structure of polyamide 6: A flash-DSC study. *Thermochim. Acta* **2017**, *657*, 110–122. [[CrossRef](#)]
76. Seguela, R. Overview and critical survey of polyamide6 structural habits: Misconceptions and controversies. *J. Polym. Sci.* **2020**, *58*, 2971–3003. [[CrossRef](#)]
77. Khanna, Y.P.; Kuhn, W.P. Measurement of crystalline index in nylons by DSC: Complexities and recommendations. *J. Polym. Sci. Part B Polym. Phys.* **1997**, *35*, 2219–2231. [[CrossRef](#)]
78. Heinrich, M.; Decker, R.; Reindel, P.; Böttcher, K.; Roth-Panke, I.; Kroll, L. Effect of acoustic excitation on fiber-reinforced polypropylene and the influence on melt viscosity. *Int. J. Adv. Manuf. Technol.* **2021**, *117*, 2395–2403. [[CrossRef](#)]

**Disclaimer/Publisher’s Note:** The statements, opinions and data contained in all publications are solely those of the individual author(s) and contributor(s) and not of MDPI and/or the editor(s). MDPI and/or the editor(s) disclaim responsibility for any injury to people or property resulting from any ideas, methods, instructions or products referred to in the content.